ACS OMEGA

http://pubs.acs.org/journal/acsodf

Article

A New Way to Predict the Efficiency of Optical Limiters without Providing an Experiment: Processing of TDDFT Calculations for the Case of Pure Two-Photon Absorption

Alexander Yu. Tolbin,* Mikhail S. Savelyev, Alexander Yu. Gerasimenko, and Victor E. Pushkarev

Cite This: *ACS Omega* 2022, 7, 28658−28666

Read Online

ACCESS | Metrics & More | Article Recommendations | Supporting Information

ABSTRACT: Laser-power-limiting devices play a predominant role in photonics because of their potential for protecting human eyes and optical devices that are sensitive to intense laser beams. This paper describes a new methodology for predicting the efficiency of optical limiting based on electric-field-induced changes in absorption spectra calculated with the TDDFT quantum-chemical method. Analytical equations are derived to evaluate the optical thresholds and speed of switching on, the dynamic range, and the degree of nonlinear attenuation of the radiation fluxes for the case of two-photon absorption. Thus, the researcher does not need to conduct costly experiments to evaluate the suitability of nonlinear absorbers for the creation of optical limiters. The possibility of developing a forecasting model is demonstrated by an example of a series of stable slipped-cofacial phthalocyanine J-type dimers, which were synthesized and investigated previously.

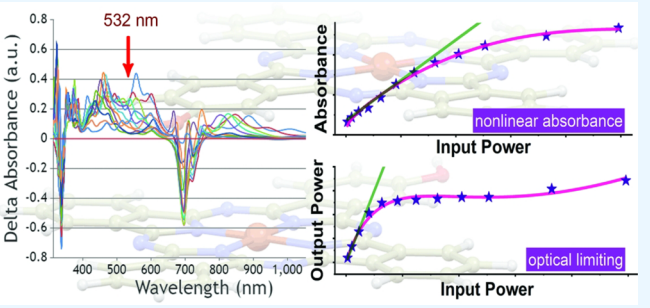

1. INTRODUCTION

The optical limiting effect is due to the nonlinear attenuation of the power, energy, or radiation flux transmitted by an optical system to a certain fixed value regardless of the magnitude of the input signal.[1,2] At the same time, the absorbing material of the optical limiter must have high transmittance at low input radiation powers.[3,4] This result is commonly used in the development of devices for protecting sensitive optical sensors from damage by laser radiation and controlling or stabilizing laser radiation in various optical logical systems.[5−7] Optical limiting is caused by nonlinear effects in the interaction of intense light with an absorbing medium, such as nonlinear absorption, refraction, scattering, and optically induced phase transitions.[8,9] Among these mechanisms, nonlinear absorption is considered when organic materials with an extended π-system (for example, phthalocyanines and related dyes) are considered since it directly affects the transmission, causing it to decrease at high levels of input radiation intensity.[10] This is because the laser radiation leads to saturation of excited states, and the dye molecule exhibits the so-called reverse saturable absorption (RSA) effect.[11,12] For phthalocyanines, this effect is observed in the range of 400−600 nm, in which most known lasers operate. The best optical limiter should have a low power-on threshold and attenuate radiation to a fixed level.

In the experiment, the optical limiting effect is observed as a decrease in transmission on the growth of the radiation power, when the sample is placed at the focus of a collecting lens.[13,14] At the same time, it was shown that the optical effect observed in laser experiments can be reproduced using *ab initio* calculations.[15] For this purpose, TDDFT calculations are performed by perturbing the ground state with electric fields polarized in all Cartesian directions.[16] Thus, the electrical component of laser radiation is associated with a series of electric fields in simulation. The calculated absorption spectra of isolated organic dyes under different electric fields demonstrate significant variation in the spectral region of transparency. The simulated optical response as the "transmittance *vs.* field strength" relationship shows a tendency toward optical limiting similar to what is usually observed in practice.[15−17] To bring theory and practice closer together, primarily, one should compare the oscillation strength of the TDDFT transitions and the absorption coefficient of the dyes in solution or a matrix. Then, one can operate with such macroscopic parameters as linear transmission and optical layer thickness. Finally, to calculate the parameters responsible for the efficiency of optical limiting, it is necessary to derive a series of analytical mathematical expressions. In the future, this will make it possible to utilize chemical structures to predict the efficiency of laser radiation limiting without conducting costly experiments.

Received: June 23, 2022
Accepted: July 20, 2022
Published: August 1, 2022

© 2022 The Authors. Published by American Chemical Society

This article is devoted to solving the above-mentioned theoretical problem for the case of pure two-photon absorption (2PA), which we previously implemented to calculate the nonlinear absorption coefficient and optical limiting response for the series of stable slipped-cofacial phthalocyanine J-type dimers (Figure 1).[18]

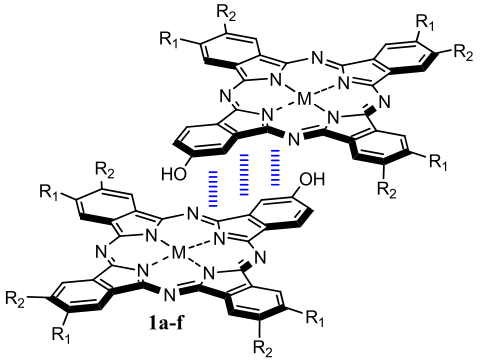

R_1/R_2 = H / *tert*-butyl;
M = 2H (**a**), Mg (**b**), Zn (**c**), Cu (**d**), Ni (**e**), Co (**f**)

Figure 1. Common chemical structure of slipped-cofacial phthalocyanine J-dimers.

2. METHODS

2.1. Quantum-Chemical Calculations. Initially, structures of the dyes **1a−f**,[16,18] in which the *tert*-butyl substituents were replaced with hydrogen atoms, were fully optimized using density functional theory (DFT) implemented in the quantum-chemical program PRIRODA[19] without solvent effects and symmetry constraints. The gradient-corrected exchange-correlation Perdew, Burke, and Ernzerhof (PBE) functional,[20] as well as the cc-pVDZ basis set[21] were utilized for this purpose. The efficient resolution of identity and parallel implementation of evaluating both Coulomb and exchange-correlation integrals with optimized fitting Gaussian basis sets in the PRIRODA code permits the performance of calculations of the molecular systems with a large number of basis functions.[19,21] A large integration grid (which comprises about 8×10^5 points over calculated molecules) with a 5×10^{-8} accuracy parameter of the adaptively generated grid was used. This parameter is responsible for the precision of the exchange-correlation energy per atom. The 10^{-6} threshold on the orbital gradients at the energy calculations tag and 10^{-5} threshold on the molecular gradient at the geometry optimization procedure were employed. The valence shells were described by basis sets with the following contraction schemes: {6s2p}/[2s1p] on H; {10s7p3d}/[3s2p1d] on C, N, and O; {14s11p6d}/[5s4p2d] on Mg; and {19s15p11d5f}/[6s5p3d1f] on Co, Ni, Cu, and Zn atoms, respectively. The vibrational analysis confirmed whether the optimized geometries correspond to local minima without imaginary frequencies.

Further, the level of theory for the optimized dimers **1a−f** was raised by including Grimme's dispersion correction. Pure DFT GGA functional B97-D and 6-31 + G(d) basis sets were utilized to perform calculations on the GAMESS-US Software[22] to re-optimize the target structures. Functional B97-D belongs to one of the most accurate general-purpose GGAs. The performance for noncovalently bound systems including many pure van der Waals complexes is exceptionally good, reaching on the average CCSD(T) accuracy.[23] In turn, the 6-31 + G(d) basis set contains diffuse and polarization functions that are required to determine the convergence of the finite field property.[24] The polarizable continuum model (PCM) was used to control the solvent effect computations (solvent − THF). The optimized structures and general computed data are presented in Section 4.1.

To study the influence of the electric fields on the electronic transitions, the linear-response time-dependent density functional theory (LR-TDDFT) implemented in GAMESS-US Software was utilized. Thus, each molecule is placed in a constant in time and uniform in space external electric field, which is included in the Schrödinger equation for the ground state,[25] followed by the calculation of the energies of excited states and oscillator strengths. Here, we assume that the action of electric fields on molecules is short-lived in time and does not cause geometric changes. The described methodology subsequently allowed us to obtain strict correlations of theoretical and experimental data regarding the parameters of optical limiting.

The resulted TDDFT spectra for each absolute value of field were obtained by the simple accumulation of all transitions in an array, followed by executing a fit with the Lorentz function $L(x)$ according to the formula

$$L(x) = \frac{1}{\pi} \sum_i \frac{w_i}{(x - x_i)^2 + w_i^2} \quad (1)$$

in which w_i is the line half-width, and x_i is the position of the electronic transitions. The variable line half-width (in the range of 0.05−0.3 eV), stretch coefficient (1.15−1.2), and a displacement factor (+*ca.* 25 nm) were used for fitting the calculated spectra to the experimental ones[18] by applying the Spectroscopy module for EasyQuanto.[26] This is necessary to most accurately predict the shape of the spectra under the action of electric fields of different intensities on the dye molecules. All quantum chemical calculations were performed on an Intel/Linux cluster (Joint Supercomputer Centre of the Russian Academy of Sciences − http://jscc.ru). Visualization of the optimized structures (Figure 4) was performed with the Mercury program obtained from the Cambridge Crystallographic Data Centre (http://ccdc.cam.ac.uk).

2.2. Analytical Calculations. *2.2.1. Conversion of Electric Field to Power.* The absolute value of the field strength in the quantum chemical programs is given in a.u. (1 a.u. = 5.14×10^{11} V m^{-1}). The series of fields F was associated with the electric component of model laser radiation and converted to power units P (Wcm^{-2}) according to the following formula

$$P = \frac{2cd_A{}^2F^2\varepsilon_0 n}{d_L{}^2} \quad (2)$$

where c is the speed of light in a vacuum, n is the refractive index of the medium (for THF, n = 1.408), ε_0 is the vacuum permittivity ($\varepsilon_0 = 8.85 \times 10^{-12}$ F m^{-1}), F is the field intensity (in V m^{-1}), d_A is the average diameter of the aggregate absorbing the light, and d_L is the laser spot diameter that is focused on the sample. Thus, we imagine an aggregation model when a homogeneous electrical induction encompasses a sphere in which the absorber molecules are enclosed and under the assumption that the aggregate exhibits the properties of a single isolated molecule. Further, we will assume that the energy of the model radiation is concentrated in a focused laser beam that passes through the aggregate, modifying its spectral character-

https://doi.org/10.1021/acsomega.2c03928
ACS Omega 2022, 7, 28658−28666

istics. This hypothesis has allowed correlating the simulation results with the experiment.

2.2.2. Processing TDDFT Spectra. The intensities of the electronic transitions in the framework of TDDFT are expressed as oscillator forces, f_{osc}, theoretically related to the probability of these transitions occurring. To compare the f_{osc} values with intensities of the experimental bands, we introduced a macroscopic coefficient D_F, the density factor of the medium, according to the following equation

$$-\ln T_0 = \alpha \times d = f_{osc} \times D_F \quad (3)$$

in which T_0 is the linear transmission, α is the linear absorption coefficient (cm^{-1}),

and d is the layer thickness (cm).

The density factor is a dimensionless quantity. For each model structure, D_F was computed by an iterative procedure. First, a sequence of D_F values from 1 to 0 was formed with a step of 0.02. Then, the absorption curves (eq 4) were calculated to evaluate α in the framework of the pure 2PA absorption model (see Section 3). In this way, a correlation between D_F and T_0 was established. The density factor was assumed to be constant for all sets of electric fields in the series.

For the numerical calculations, analytical wavelength and T_0 were set to 532 nm and 0.7, respectively, as in the experiment.[18] In this way, we can establish the relationship between the calculated TDDFT spectra and the molar concentration of the sample.

3. THEORETICAL BACKGROUND

Since the relationship between absorption and the external fields can be nonlinear, we used the following nonlinear function

$$k(x) = \frac{c}{b}\left(1 + \frac{(\ln(x) - a)^2}{b^2}\right)^{-1} \quad (4)$$

in which a, b, and c are the fitting parameters.

This is a modified Cauchy's distribution[27] represented as the smooth, continuous, and infinitely differentiable function for all $x > 0$. This function allows deriving all the required analytical expressions in a simple and understandable form. However, for the 2PA absorption model, a linear relationship between absorption and radiation power is assumed.[18] Therefore, we expand $k(x)$ into the Taylor series, truncating high-order terms:

$$k(x) = \alpha + \beta x \quad (5)$$

where β is the effective nonlinear two-photon absorption coefficient.[28,29] The proposed approach allows one to derive equations for three-photon (3PA), mixed (2 + 3) PA, and other absorption models of any complexity. The optical limiting properties of dyes **1a**–**f** were previously investigated in the framework of the 2PA absorption model at the 532 nm wavelength by applying nanosecond laser radiation (16 ns pulses).[18] In this way, we can establish the correlation between simulation and experiment (Section 4.3.).

The optical limiting curves (output signal) relate the output radiation flux with the input radiation, according to the equation

$$T(x) = \exp(-k(x) \times d) \quad (6)$$

in which $T(x)$ is the transmission which depends on the intensity of the external influence: $T(x) = x_{out}/x$. The appearance of such curves is largely determined by the total absorption coefficient $k(x)$. Depending on the linear transmission T_0, three types of curves can be observed corresponded to blacking-out ($T_0 < 0.5$), limiting ($0.5 < T_0 < 0.8$), and (non)linear ($T_0 > 0.8$) attenuation of the input radiation. In the first and last cases, the absorber can be used as a radiation interrupter and a light filter, respectively.

3.1. Nonlinear Absorbance. Absorbance at a wavelength of 532 nm, being typical for providing laser experiments, demonstrates a nonlinear pattern concerning the strength of external electric fields (recall that we are considering the intensity of laser radiation, implying only its electrical component). The fitting of calculated absorbance with eq 4 gives the smoothed curves ($R^2 > 0.9$). Deviation from linearity is observed at high values of electric fields, which can be associated with an orbital distortion.[30,31] This, in turn, leads to disturbing the distribution of electron clouds involved in orbitals, which results in a higher overlap during electron transitions.[32] For this reason, in simulations, we have a picture similar to multiphoton absorption, which is observed in laser experiments.

Next, we need to cut off nonlinearity to follow the 2PA absorption model.[16,18] Differential analyses of eq 4 have indicated two characteristic points on the absorption curves. The first, P_{NL}, corresponds to the start of nonlinear processes, and the second corresponds to the saturation of absorption, P_D:

$$\frac{1}{k}\frac{d^2k}{dt^2} = \frac{-2b^2 + 6(a - t)^2}{(b^2 + (a - t)^2)^2} \quad (7)$$

where $t = \ln(x)$.

The chart of the eq 7 in linear coordinates is shown in Figure 2 with a violet line.

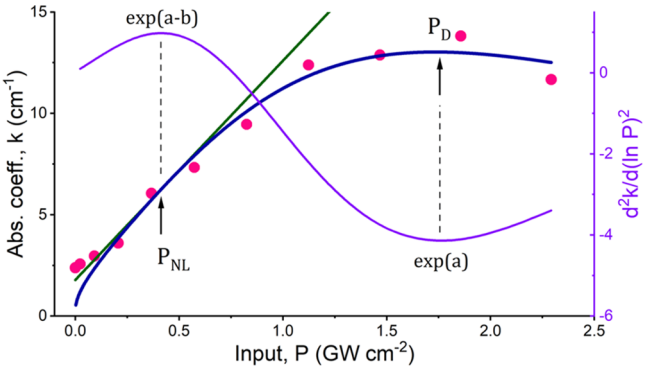

Figure 2. Nonlinear absorption of dye **1c** under different electric fields applied: TDDFT calculated spectral response is displayed with red dots; the blue and violet curves represent fittings corresponding to eqs 4 and 7, respectively. The optical pathlength and linear transmission at 532 nm were set to 0.2 and 0.7 cm, respectively. The 2PA absorption model fit is shown with a green line (eq 8). P_D is the saturation of absorption, followed by bleaching, or optical breakdown of the absorber. Point P_{NL} corresponds to the deviation of absorbance from linearity.

The extrema of d^2k/dt^2 are marked on the charts: maximum, $P_{NL} = \exp(a - b)$, and minimum, $P_D = \exp(a)$. Let us expand eq 4 in a Taylor series in powers of $n = 1$ in the vicinity of the point P_{NL}:

$$k_{2PA}(x) = \frac{(-1 + b)c}{2b^2} + \frac{e^{-a+b}c}{2b^2} \times x = \alpha + \beta x \quad (8)$$

From the absorption curves, most parameters can be derived for assessing the effect of laser radiation on dyes (Table 1, eqs 9–14). However, there are still limiting thresholds that are also

https://doi.org/10.1021/acsomega.2c03928
ACS Omega 2022, 7, 28658–28666

Table 1. General Derived Parameters Based on the Applied Pure 2PA Absorption Model to Evaluate the Optical Limiting Properties of Dyes 1a−f[a]

parameter	equation (eq no.)
Calculated from absorption curves (k *vs.* input power)	
linear absorption coefficient	$\alpha = \frac{(-1+b)c}{2b^2}$ (9)
nonlinear two-photon absorption coefficient	$\beta = \frac{e^{-a+b}c}{2b^2}$ (10)
linear transmission (d is the optical pathlength)	$T_0 = \exp\left(-\frac{(-1+b)cd}{2b^2}\right)$ (11)
optical destruction of the absorber	$P_D = e^a$ (12)
transmission at the P_D	$T_D = e^{-cd/b}$ (13)
attenuation coefficient	$k_A = \frac{T_0}{T_D} = \exp\left(\frac{(1+b)cd}{2b^2}\right)$ (14)
Calculated from output curves (output *vs.* input power)	
point of deviation from T_0 on the output curve (limiting threshold)	$P_0 \cong \frac{0.0760}{\beta d}$ (15)
point of completion of deviation from linearity	$P_1 = \frac{1}{\beta d}$ (16)
limiting threshold for the ideal optical limiter	$P_L = \frac{1}{e\beta d} \cong \frac{0.3681}{\beta d}$ (17)
dynamic range of the limiter	$DR = P_D/P_0$ (18)
limiter activation speed	$r \cong 1.9397\sqrt{e^{2+\alpha d}}\beta d$ (19)

[a] a, b, and c are the fitting parameters of eq 4.

important for evaluating the effectiveness of optical limiters. We will search for them based on the analysis of the limiter curves.

3.2. Optical Limiting Effect. At high fields, dyes **1a−f** show a drop in absorption observed a little before the saturation point P_D (Figures 2 and 3). We call this point the limiter destruction threshold. At $P > P_D$, the limiter curves deviate upward, which in terms of a laser experiment represents the optical breakdown of the material. In Figure 3b,c, the area of the possible destruction of the material is shown with a dashed line. This result is partially consistent with the deviation from the applied pure 2PA absorption model (eq 4) describing the overall process.

Destruction point P_D (eq 12) is important for calculating the dynamic range of optical limiters. However, first of all, it is necessary to find on the limiter curve the point of deviation (P_0) of the transmission from the given linear value at the irradiation wavelength. To do this, we switch to logarithmic coordinates by the argument ($x = e^t$) and process a differential analysis. To simplify the expressions, we will work with eq 5. In logarithmic coordinates for the case of two-photon absorption, the limiter curve will be described by the following expression:

$$y = \exp(t - d(\alpha + e^t\beta)) \quad (20)$$

The derivatives of eq 20 for t are represented as

$$\frac{1}{y}\frac{d^n y}{dt^n} = 1 + \sum_{i=1}^{n} A_i(e^t\beta d)^i \quad (21)$$

That is, they are polynomials of the n^{th} degree by the argument e^t($= x$). Functions $d^n y/dt^n$ have extrema. The first of these is always the maximum, and it makes practical sense, while the

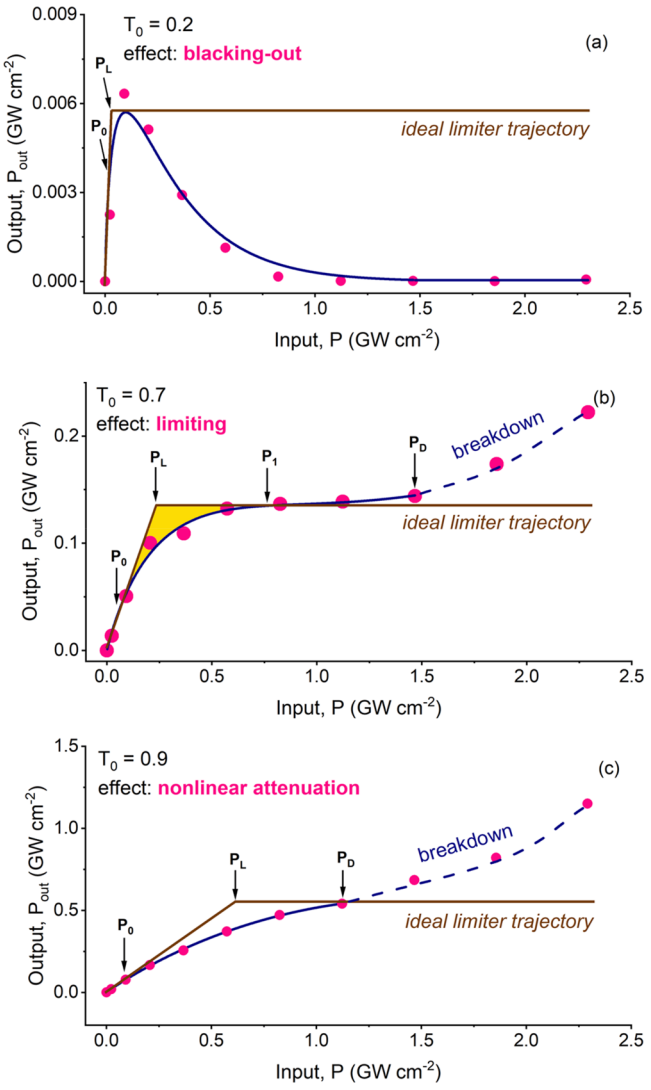

Figure 3. TDDFT simulation of some possible effects of the interaction of laser radiation with an absorber for different linear transmission values (an example for dye **1c**): blacking-out (a), limiting (b), and nonlinear attenuation (c). The trajectory of an ideal limiter is shown with a brown line. Localization of points P_0, P_1, P_D, and P_L (Table 1) was performed according to eqs 12 and 15−17. The pure 2PA absorption model (eqs 6 and 8) was utilized to fit output curves (blue solid lines). Deviation from the applied model is indicated with a broken line. The yellow background in (b) shows the area responsible for the speed of the limiter activation.

others are not. The solution of equations $\frac{1}{y}\frac{d^n y}{dt^n} = 0$ for $n > 2$ is possible only numerically, and this gives the position of the potential point of deviation of the output signal from the linear transmission, *i.e.*, limiting threshold (P_0). The larger the n, the closer to zero this point tends. In general form, the solutions of these differential equations can be written as follows:

$$x = \frac{m}{\beta d} \quad (22)$$

where m is a real number ($m \leq 1$). For $m = 1$, we have a position of point P_1 (eq 16)—the completion of deviation from linearity, which is blurred in a certain interval of input energies. To localize the point P_0 on the limiter curve, we introduce the parameter ξ, the absolute deviation of two functions: linear

https://doi.org/10.1021/acsomega.2c03928
ACS Omega 2022, 7, 28658−28666

transmission ($y = T_0x$) and nonlinear attenuation (eq 6) at the point $x = x_0$. The equation

$$\frac{e^{-(m+\alpha d)}(-1 + e^m)m}{\beta d} \leq \xi \tag{23}$$

cannot be solved analytically for m, but the expression for the relative error δ looks much simpler:

$$1 - e^{-m} < \delta < -1 + e^m \tag{24}$$

Here, $m \to 0$: $\delta \to m$. For $m = 0.0760038$ (the first extremum of the function d^3y/dt^3),

$\overline{\delta} \approx 0.0760770$. Such accuracy is quite enough for us to determine the deviation threshold P_0, and this does not contradict visual control (see eq 15 and Figure 3). The ideal limiter curve is another indicator of the effectiveness of an absorber in optical limiting. Comparison with the real curve shape allows judging how quickly the limiter "turns on". This is important for instantaneous protection operation. The limiting threshold for the ideal limiter, P_L, is calculated by eq 17; it is located at the intersection of two tangents marked in Figure 3 with brown lines. It is important to note that the thresholds P_0 and P_L are dependent on the nonlinear response of the material. The higher the β, the lower the thresholds, and therefore, at lower input radiation fluxes, the limiter starts to work. In turn, the rate at which the limiter is turned on (eq 19) is directly proportional to β and also depends on linear absorption (*i.e.*, concentration). However, a significant increase in α results in darkening (Figure 3a). Therefore, the issue of concentration and aggregation of dyes requires special attention along with their nonlinear properties.

The mathematical details regarding this section can be found in the Supporting Information. All analytical mathematical calculations were carried out with the Wolfram Mathematica 10.0 suite (https://wolfram.com/mathematica).

4. RESULTS AND DISCUSSION

4.1. DFT Structures. The DFT optimized structures of dyes **1a**−**f** are shown in Figure 4. As we noted in ref 17, slipped-

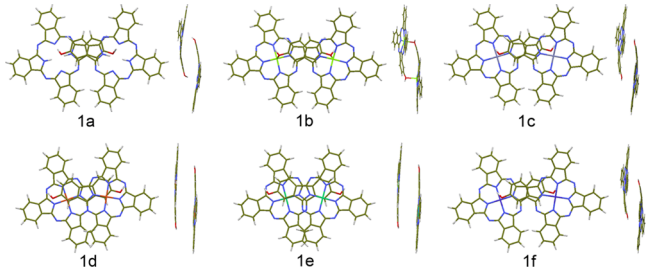

Figure 4. DFT (B97-D/6-31 + G(d))-optimized structures of phthalocyanine J-type dimers. *tert*-Butyl substituents were replaced with hydrogen atoms to reduce calculation time.

cofacial phthalocyanine J-type dimers can exist as two isomers—parallel and oblique. These isomers belong to different symmetry groups; they are formed with equal probability in syntheses, but the composition of the mixtures cannot be easily controlled. The oblique isomer belongs to the C_2 symmetry group, while the parallel isomer belongs to the C_i group. In the latter case, the structure has an inversion center, and therefore, second-order nonlinear optical properties are not realizable for it. Adjusting the parallel/oblique ratio in prospect will selectively control the magnitude of the second order nonlinear response. The isomerism of J-type cofacial dimers was first revealed by Kazuya *et al.* on the example of imidazolyl-substituted phthalocyanines.[33]

Structures of J-dimers **1a**−**f** are characterized by the distortion of macrocycles, which prevents the aggregation of molecules in solutions and the solid phase. As a result, the ordered structures are formed.[16]

4.2. Optical Limiting Effect and Absorption Efficiency. In the present investigation, we assume that under the action of external fields, a molecule passes into excited metastable states, the lifetime of which is rather long compared to a light pulse. As the intensity of the external fields increases, the dipole-forbidden levels are populated in the visible region, and these electronic transitions contribute to the total absorption, enhancing it. It has been demonstrated that such an assumption leads to correctly reproducing the trend and the overall shape of the optical limiting fingerprint.[15] Placing a molecule in a strong electric field opens up exciting nonperturbative phenomena such as inconsistent multiple ionization, the origins of which lie in the subtle ways of interaction of electrons with each other. The potential of external electric fields is added to the Hamiltonian, and then the time-dependent Schrödinger equation is solved for the many-electron wavefunctions.[25] The applied electric fields induce charge transfer in the molecules, with the dipole moment of the molecule changing linearly at smaller fields and exponentially otherwise.[35]

The calculated TDDFT spectra of the model phthalocyanine J-dimers **1a**−**f** under electric fields applied are shown in Figure 5. The response is presented in ΔA units: $\Delta A = A(F) - A(F = 0)$ to demonstrate the possible occurrence of the optical limiting effect ($\Delta A > 0$), which is detected in a wide range of wavelengths. J-dimers **1a**−**f** may be of interest as nonlinear absorbers in the 400−600 and 750−850 nm ranges where transparency is observed in the absence of incident radiation. At a wavelength of 532 nm (the second harmonic of an Nd: YAG laser), the absorption density for most dyes is high, which explains the good optical limiting response that we observed earlier.[18] However, nickel (**1e**) and cobalt (**1f**) complexes demonstrate low efficiency due to poor absorbance density at 532 nm.

With an increase in the strength of the electric field, the absorption response increases nonlinearly. However, in this study, we are restricting with a pure two-photon absorption model, which can be applied only for weak fields (0.001−0.005 a.u.). A deviation from this model allows finding the switch-on point (P_1, eq 16) on the limiter curve, after which an almost stationary response of the absorber to the external impact follows. Saturation absorption is the maximum on the absorption curve; further (at even stronger fields), a drop in absorption is possible, and this means an optical breakdown of the material (Figure 3c).

A more detailed consideration of the influence of electric fields on the nonlinear properties of molecules in TDDFT calculations will require the use of complicated models, in particular, (2 + 3) PA, for which it is necessary to add a quadratic term in eq 5 or, say, removing linearity ($\beta = 0$), leaving only nonlinear terms. In our further works, we will pay attention to evaluating the contribution to limiting multiphoton processes, which can be simulated by using strong fields in calculating electronic transitions.

4.3. Correlations. Applying the factor analysis of the data presented in Table 2 has allowed us to solve a multiparametric problem and simulate the relationship between the optical

https://doi.org/10.1021/acsomega.2c03928
ACS Omega 2022, 7, 28658−28666

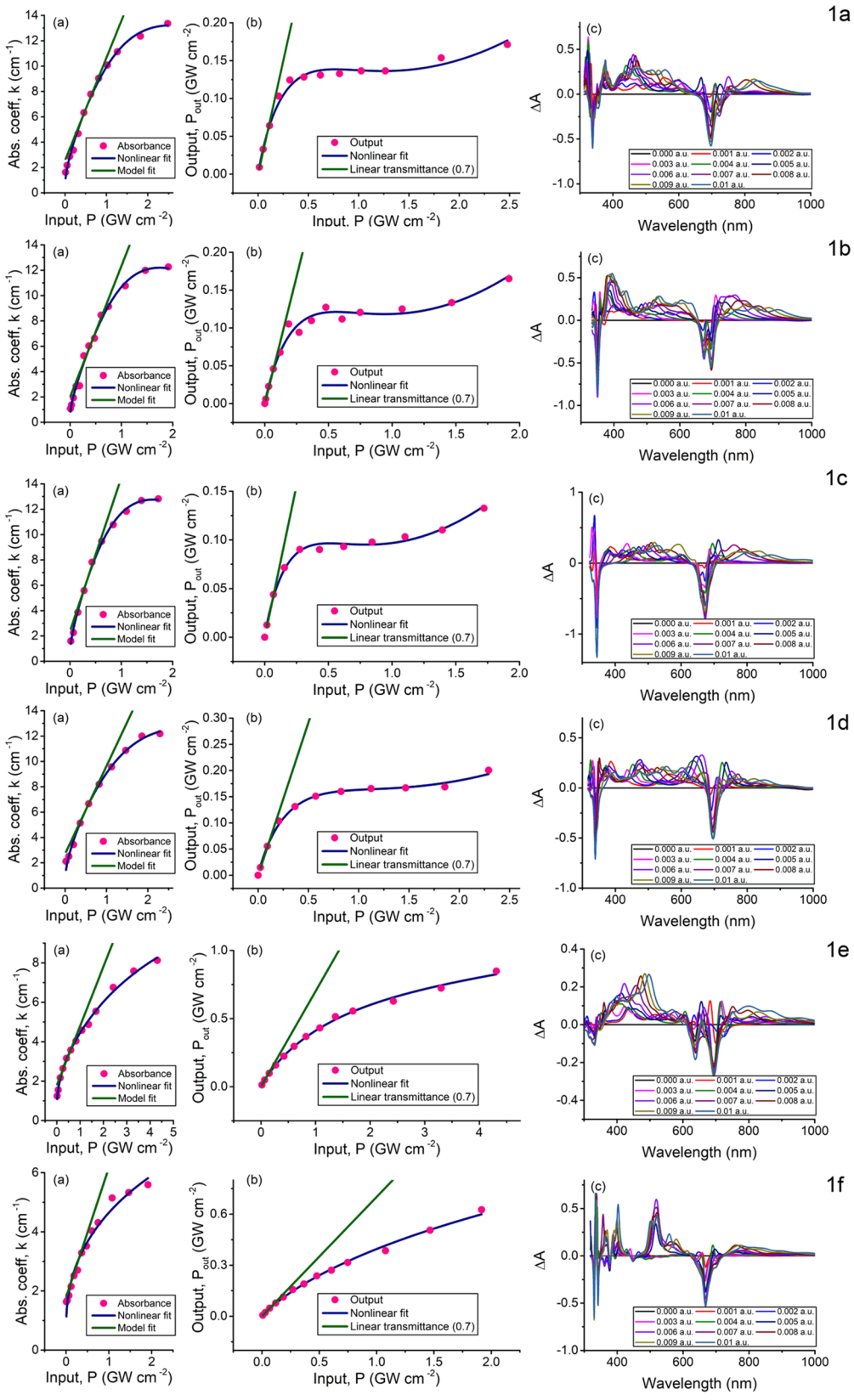

Figure 5. TDDFT simulation (B97/6−31 + G(d)) of nonlinear absorbance (a) and optical limiting output signal (b) based on the calculated electroabsorption spectra (c) of phthalocyanine J-dimers **1a**−**f**. The optical pathlength and linear transmittance at the analytical wavelength (532 nm) were set to 0.2 cm and 0.7, respectively.

limiting parameters calculated by quantum-chemical modeling of nonlinear absorption and the ones obtained experimentally. Experimental and simulation data were used as dependent and independent variables, respectively. Employing a multi-iterative

https://doi.org/10.1021/acsomega.2c03928
ACS Omega 2022, 7, 28658−28666

Table 2. General Computed Data for the Structures of Dimeric Phthalocyanines 1a–f and Experimental Data of the Nonlinear Properties of these Dyes[a]

	dyes					
parameter	1a	1b	1c	1d	1e	1f
Optimized structures (B97-D/6-31 + G(d))						
angle of slippage (deg)	24.1	21.2	22.4	23.8	36.5	20.8
tilt angle (deg)	3.9	17.1	13.2	4.1	1.1	12.9
relative rotation of the macrocycles (deg)	46.2	47.3	50.5	49.3	40.8	48.2
distance between macrocycles (Å)	4.8	3.8	3.9	3.8	3.8	3.9
Experimental data						
average size of aggregates (nm)[34] (for substitution in eq 2)	53	124	105	116	131	70
radius of the laser beam in focus (μm)[18] (for substitution in eq 2)	64	67	64	68	48	64
nonlinear two-photon absorption coefficient (β, cm GW^{-1})[18]	315	340	360	228	57	21
limiting threshold (P_0, GW cm^{-2})[18]	0.03	0.05	0.03	0.03	0.65	0.60
dynamic range of the limiter (DR)[18]	1000	460	830	930	72	82
attenuation coefficient (k_A)[18]	8.0	7.0	7.8	6.4	3.2	1.7
simulation[b]						
nonlinear two-photon absorption coefficient (β, cm GW^{-1}), eq 10	8.09	10.31	12.12	6.93	3.01	2.38
optical destruction (P_D, GW cm^{-2}), eq 12	2.56	1.75	1.62	2.99	15.38	19.70
attenuation coefficient (k_A), eq 14	8.41	7.71	8.01	7.33	4.77	3.65
limiting threshold (P_0, GW cm^{-2}), eq 15	0.04	0.04	0.03	0.05	0.25	0.21
dynamic range of the limiter (DR), eq 18	52.5	54.6	51.6	54.6	70.1	78.3
limiter activation speed (R, cm^2 W^{-1}), eq 19	11.0	13.3	16.2	9.6	2.2	2.3

[a]Nd: YAG laser source; linear transmittance, 0.7 at 532 nm analytical wavelength; solvent, THF; concentration, ca. 2.3 × 10^{-4} mol L^{-1}; optical pathlength, 0.2 cm. [b]Based on equations from Table 1.

procedure of combining regressors implemented in the Correlato program,[36] strict correlations with experiments are found for the development of a forecasting model. Thus, having at their disposal only the structure of a substance, a researcher can figure out (1) whether this compound is capable of giving the optical limiting effect and (2) what the nonlinear response will be in practice. In other words, within the framework of a given model, with some approximation, it is possible to obtain experimental data without performing a costly experiments.

Figure 6 shows the result of the multivariate regression analysis. Thus, for the nonlinear absorption coefficient β and the radiation attenuation coefficient k_A, the correlations are linear ($R^2 > 0.98$), while for the limiting threshold P_0 and the dynamic range DR, we failed to obtain a linear response. Perhaps this is due to the accuracy of their estimation in the experiment. In particular, to calculate the DR, it is necessary to know the exact value of the radiation energy destroying the limiter material, and it can be determined only approximately since the medium in which the absorber is placed also exhibits nonlinear properties at high input energies. The speed of switching on the limiter, r, is included in all correlation expressions (Figure 6). The exclusion of this variable from the analysis greatly worsens the sought relationships. The highest values of r were found for zinc J-dimer **1c** (16.2 cm^2 W^{-1}). The worst result was obtained for the nickel (**1e**) and cobalt (**1f**) complexes (~2 cm^2 W^{-1}). This is due to the low degree of π–π interactions of macrocycles in these dimeric structures compared to other complexes. Although dyes **1e,f** are more resistant to laser radiation, it is impractical to use them as optical limiters.

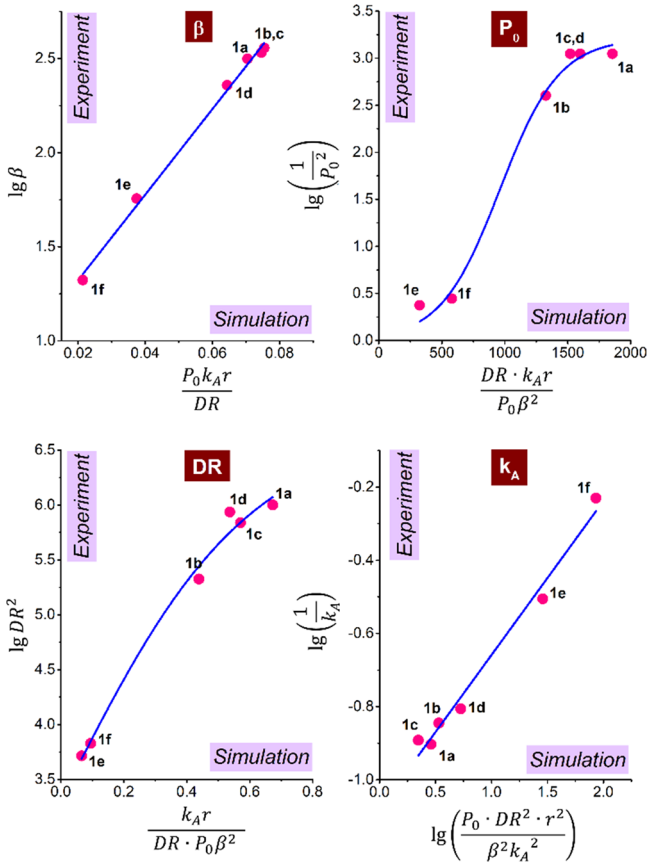

Figure 6. Experiment *vs.* simulation correlations for the nonlinear absorption coefficient β (cm GW^{-1}), limiting threshold P_0 (GW cm^{-2}), dynamic range DR, and attenuation coefficient k_A.

5. CONCLUSIONS

Thus, in this study, we have implemented an integrated approach aimed at quantifying the efficiency of optical limiting based on TDDFT calculations. Having only an optimized structure, first, the researcher, can reveal whether the nonlinear absorber is capable of demonstrating the optical limiting effect. Further, having chosen a certain standard, one can evaluate the relative efficiency of the optical limiting. However, for creating

https://doi.org/10.1021/acsomega.2c03928
ACS Omega 2022, 7, 28658–28666

the forecasting model to obtain experimental values (with a certain degree of reliability) without providing experiments, it is still necessary to conduct laser experiments for a small series of similar absorbers under given conditions and build correlations. Obviously, the wider the series, the more accurate the prediction will be. Thus, the correlations between theory and experiment will provide the numerical result for some derivatives.

Numerical processing of TDDFT spectra is greatly simplified if a pure two-photon absorption model is used, resulting in cutting off the unnecessary nonlinearity in absorption caused by strong electric fields, especially since this nonlinearity leads to bleaching in simulation (Figure 3b,c) or optical breakdown in practice. However, using our approach, the researcher can derive similar equations, for example, for the case of pure three-photon or even multiphoton absorption, since the Taylor series expansion of absorption nonlinear function (in this work eq 4) can be done with any number of terms.

We have implemented an indirect method for simulating the optical limiting effect, which is based on the calculation of absorption spectra with external electric fields that simulate the laser irradiation. This approach, firstly described by Cocchi *et al.*,[15] has the advantage that the researcher does not need to characterize all the phenomena occurring at the interaction of intense light with the substance; it is general and is not limited to phthalocyanines since TDDFT spectra can be calculated for each structure in the presence of electric fields. Also, it does not matter how many electrons a molecule has or whether it has an open or closed shell structure, since the TDDFT and finite field DFT methods are equally applicable to all structures. Only the calculation time can serve as a limitation since it is necessary to solve a large number of quantum-chemical tasks.

■ ASSOCIATED CONTENT

Supporting Information

The Supporting Information is available free of charge at https://pubs.acs.org/doi/10.1021/acsomega.2c03928.

Detailed mathematical calculations regarding the derivation of the equations from Table 1 based on absorption and limiter curves (PDF)

■ AUTHOR INFORMATION

Corresponding Author

Alexander Yu. Tolbin − *FSBIS Institute of Physiologically Active Compounds of the Russian Academy of Sciences, Russian Academy of Sciences, 142432 Moscow, Russian Federation;* orcid.org/0000-0002-5541-5401; Phone: +7 496 5242566; Email: tolbin@ipac.ac.ru

Authors

Mikhail S. Savelyev − *National Research University of Electronic Technology Institute of Biomedical Systems, 124498 Moscow, Russian Federation; I.M. Sechenov First Moscow State Medical University Institute of Regenerative Medicine, 119991 Moscow, Russian Federation*

Alexander Yu. Gerasimenko − *National Research University of Electronic Technology Institute of Biomedical Systems, 124498 Moscow, Russian Federation; I.M. Sechenov First Moscow State Medical University Institute of Regenerative Medicine, 119991 Moscow, Russian Federation*

Victor E. Pushkarev − *FSBIS Institute of Physiologically Active Compounds of the Russian Academy of Sciences, Russian Academy of Sciences, 142432 Moscow, Russian Federation;* orcid.org/0000-0003-3984-1061

Complete contact information is available at: https://pubs.acs.org/10.1021/acsomega.2c03928

Notes

The authors declare no competing financial interest.

■ ACKNOWLEDGMENTS

The main research was carried out with the financial support of the Russian Science Foundation (grant 21-73-20016). A study of the NLO properties of ligand **1a** was carried out by analogy with metal complexes **1b−f** presented in ref 18 within the framework of the State Assignment of 2022 (Theme 45.5, Creation of compounds with given physicochemical properties, no. FFSN-2021-0003). The authors also thank the Joint Supercomputer Centre of RAS (www.jscc.ru) for providing computing resources. We are especially grateful to Professor Larisa G. Tomilova, founder of the native Phthalocyanine School. Disciples and followers of Prof. L.G. Tomilova are deeply grieved over the loss of the Mentor. She passed away on 4 January 2021 at the age of 74 after enduring COVID-19 just a few weeks before the vaccine is available. This article is dedicated to her memory.

■ REFERENCES

(1) Rao, K. S.; Ganeev, R. A.; Zhang, K.; Fu, Y.; Boltaev, G. S.; Maurya, S. K.; Guo, C. Comparative Analyses of Optical Limiting Effects in Metal Nanoparticles and Perovskite Nanocrystals. *Opt. Mater.* **2019**, *92*, 366−372.

(2) Hagan, D. J.; Xia, T.; Said, A. A.; Wei, T. H.; Stryland, E. W. V. High Dynamic Range Passive Optical Limiters. *Int. J. Nonlinear Opt. Phys.* **1993**, *02*, 483−501.

(3) Qu, S.; Song, Y.; Liu, H.; Wang, Y.; Gao, Y.; Liu, S.; Zhang, X.; Li, Y.; Zhu, D. A Theoretical and Experimental Study on Optical Limiting in Platinum Nanoparticles. *Opt. Commun.* **2002**, *203*, 283−288.

(4) Baev, A.; Rubio-Pons, O.; Gel'mukhano, F.; Ågren, H. Optical Limiting Properties of Zinc- and Platinum-Based Organometallic Compounds. *J. Phys. Chem. A* **2004**, *108*, 7406−7416.

(5) Yu, C.; Lili, G.; Miao, F.; Lingling, G.; Nan, H.; Jun, W.; Yasuyuki, A.; Werner, J. B.; Osamu, I. Photophysical and Optical Limiting Properties of Axially Modified Phthalocyanines. *Mini-Rev. Org. Chem.* **2009**, *6*, 55−65.

(6) Rychnovsky, S.; Allan, G.; Venzke, C.; Smirl, A.; Boggess, T. Optical Nonlinearities and Optical Limiting in Gap at 532 Nm. *Proc. SPIE* **1692**, *1992*, 191−196.

(7) de la Torre, G.; Vázquez, P.; Agulló-López, F.; Torres, T. Phthalocyanines and Related Compounds: Organic Targets for Nonlinear Optical Applications. *J. Mater. Chem.* **1998**, *8*, 1671−1683.

(8) Rashidian, M.; Dorranian, D. Investigation of Optical Limiting in Nanometals. *Rev. Adv. Mater. Sci.* **2015**, *40*, 110−126.

(9) Lind, P. In *Organic and Organometallic Compounds for Nonlinear Absorption of Light*, Akademisk avhandling, Umeå University department of chemistry - organic chemistry: 2007; p 84.

(10) de la Torre, G.; Vázquez, P.; Agulló-López, F.; Torres, T. Role of Structural Factors in the Nonlinear Optical Properties of Phthalocyanines and Related Compounds. *Chem. Rev.* **2004**, *104*, 3723−3750.

(11) Yan, X.; Wu, X.; Fang, Y.; Sun, W.; Yao, C.; Wang, Y.; Zhang, X.; Song, Y. Ultrafast Broadband Reverse Saturation Absorption in Al-Doped Inse Thin Films for Optical Limiting at Visible/near-Infrared. *Opt. Mater.* **2020**, *108*, No. 110171.

(12) Ghaderi Goran Abad, M.; Mahdieh, M.; Veisi, M.; Nadjari, H.; Mahmoudi, M. Coherent Control of Optical Limiting in Atomic Systems. *Sci. Rep.* **2020**, *10*, 2756.

(13) Wang, Q.; Rogers, E. T. F.; Gholipour, B.; Wang, C.-M.; Yuan, G.; Teng, J.; Zheludev, N. I. Optically Reconfigurable Metasurfaces and

Photonic Devices Based on Phase Change Materials. *Nat. Photonics* **2016**, *10*, 60−65.
(14) Pan, B.; Yu, L.; Wu, D. High-Accuracy 2d Digital Image Correlation Measurements Using Low-Cost Imaging Lenses: Implementation of a Generalized Compensation Method. *Meas. Sci. Technol.* **2014**, *25*, No. 025001.
(15) Cocchi, C.; Prezzi, D.; Ruini, A.; Molinari, E.; Rozzi, C. A. Ab Initio Simulation of Optical Limiting: The Case of Metal-Free Phthalocyanine. *Phys. Rev. Lett.* **2014**, *112*, No. 198303.
(16) Tolbin, A. Y.; Dzuban, A. V.; Shulishov, E. V.; Tomilova, L. G.; Zefirov, N. S. Slipped-Cofacial J-Type Phthalocyanine Dimers as Potential Non-Linear Absorbers for Optical Limiting Applications. *New J. Chem.* **2016**, *40*, 8262−8270.
(17) Tolbin, A. Y.; Pushkarev, V. E.; Tomilovaa, L. G.; Zefirov, N. S. Monohydroxyphthalocyanines as Potential Precursors to Create Nanoscale Optical Materials. *J. Porphyrins Phthalocyanines* **2017**, *21*, 128−134.
(18) Tolbin, A. Y.; Savelyev, M. S.; Gerasimenko, A. Y.; Tomilova, L. G.; Zefirov, N. S. Thermally Stable J-Type Phthalocyanine Dimers as New Non-Linear Absorbers for Low-Threshold Optical Limiters. *Phys. Chem. Chem. Phys.* **2016**, *18*, 15964−15971.
(19) Laikov, D. N. Fast Evaluation of Density Functional Exchange-Correlation Terms Using the Expansion of the Electron Density in Auxiliary Basis Sets. *Chem. Phys. Lett.* **1997**, *281*, 151−156.
(20) Erznzerhof, M.; Scuseria, G. E. Assessment of the Perdew−Burke−Ernzerhof Exchange-Correlation Functional. *J. Chem. Phys.* **1999**, *110*, 5029.
(21) Laikov, D. N. A New Class of Atomic Basis Functions for Accurate Electronic Structure Calculations of Molecules. *Chem. Phys. Lett.* **2005**, *416*, 116−120.
(22) Schmidt, M. W.; Baldridge, K. K.; Boatz, J. A.; Elbert, S. T.; Gordon, M. S.; Jensen, J. H.; Koseki, S.; Matsunaga, N.; Nguyen, K. A.; Su, S.; Windus, T. L.; Dupuis, M.; Montgomery, J. A. General Atomic and Molecular Electronic Structure System. *J. Comput. Chem.* **1993**, *14*, 1347−1363.
(23) Grimme, S. Semiempirical Gga-Type Density Functional Constructed with a Long-Range Dispersion Correction. *J. Comput. Chem.* **2006**, *27*, 1787−1799.
(24) Maroulis, G. On the Accurate Theoretical Determination of the Static Hyperpolarizability of Trans-Butadiene. *J. Chem. Phys.* **1999**, *111*, 583−591.
(25) Gross, E. K. U.; Maitra, N. T. Introduction to TDDFT. In *Fundamentals of Time-Dependent Density Functional Theory*, Marques, M. A. L.; Maitra, N. T.; Nogueira, F. M. S.; Gross, E. K. U.; Rubio, A., Eds. Springer Berlin Heidelberg: Berlin, Heidelberg, 2012; pp. 53−99.
(26) Tolbin, A. Yu. *The Control System of the Quantum-Chemical Calculations − Easyquanto. Certificate of State Registration of Computer Program No 2015619026 (Ru)*; 2015.
(27) Sugiyama, M. Examples of Continuous Probability Distributions. In *Introduction to Statistical Machine Learning*, Sugiyama, M., Ed. Morgan Kaufmann: Boston, 2016; pp. 37−50.
(28) Gaur, A.; Syed, H.; Yendeti, B.; Soma, V. R. Experimental Evidence of Two-Photon Absorption and Its Saturation in Malachite Green Oxalate: A Femtosecond Z-Scan Study. *J. Opt. Soc. Am. B* **2018**, *35*, 2906−2914.
(29) Pramodini, S.; Deepika; Sandhya; Rao, A.; Poornesh, P. Studies on Thermally Induced Third-Order Optical Nonlinearity and Optical Power Limiting Response of Azure B under Cw He−Ne Laser Excitation. *Opt. Laser Technol.* **2014**, *62*, 58−62.
(30) Neog, B.; Sarmah, N.; Kar, R.; Bhattacharyya, P. K. Effect of External Electric Field on Aziridinium Ion Intermediate: A Dft Study. *Comput. Theor. Chem.* **2011**, *976*, 60−67.
(31) Kang, B.; Baek, K. Y.; Lee, J. Y. Electric Field Effect on Trans-P-Hydroxybenzylideneimidazolidinone: A Dft Study and Implication to Green Fluorescent Protein. *Bull. Korean Chem. Soc.* **2015**, *36*, 276−281.
(32) Xie, M.; Wang, J.; Ren, J.; Hao, L.; Bai, F.-Q.; Pan, Q.-J.; Zhang, H.-X. Theoretical Study on a High-Efficient Porphyrin-Sensitizer in a Local Electric Field: How Does the Local Electric Field Affects the Performance of Dye-Sensitized Solar Cells? *Org. Electron.* **2015**, *26*, 164−175.
(33) Kazuya, K.; Mitsuhiko, M.; Akiharu, S.; Yoshiaki, K. Highly Fluorescent Self-Coordinated Phthalocyanine Dimers. *Am. Ethnol.* **2005**, *117*, 4841−4844.
(34) Tolbin, A. Y.; Pushkarev, V. E.; Sedova, M. V.; Maklakov, S. S.; Tomilova, L. G. Aggregation of Slipped-Cofacial Phthalocyanine J-Type Dimers: Spectroscopic and AFM Study. *Spectrochim. Acta, Part A* **2018**, *205*, 335−340.
(35) Sıdır, İ.; Sıdır, Y. G.; Berber, H.; Demiray, F. Emerging Ground and Excited State Dipole Moments and External Electric Field Effect on Electronic Structure. A Solvatochromism and Theoretical Study on 2-((Phenylimino)Methyl)Phenol Derivatives. *J. Mol. Liq.* **2015**, *206*, 56−67.
(36) Tolbin, A.Yu. *Establishing Correlations between Unlimited Datasets - Correlato, Certificate of State Registration of Computer Program No 2022613888 (Ru)*; 2022.

https://doi.org/10.1021/acsomega.2c03928
ACS Omega 2022, 7, 28658−28666